

Dependence on temperature and salinity gradients and the injection rate of CO₂ storage in saline aquifers with an angular unconformity

Pourmalek, A. & Shariatipour, S. M.

Author post-print (accepted) deposited by Coventry University's Repository

Original citation & hyperlink:

Pourmalek, A & Shariatipour, SM 2019, 'Dependence on temperature and salinity gradients and the injection rate of CO₂ storage in saline aquifers with an angular unconformity' *Journal of Porous Media*, vol. 22, no. 8, pp. 1065-1078.
<https://dx.doi.org/10.1615/JPorMedia.2019025077>

DOI 10.1615/JPorMedia.2019025077

ISSN 1091-028X

ESSN 1934-0508

Publisher: Begell House

Copyright © and Moral Rights are retained by the author(s) and/ or other copyright owners. A copy can be downloaded for personal non-commercial research or study, without prior permission or charge. This item cannot be reproduced or quoted extensively from without first obtaining permission in writing from the copyright holder(s). The content must not be changed in any way or sold commercially in any format or medium without the formal permission of the copyright holders.

This document is the author's post-print version, incorporating any revisions agreed during the peer-review process. Some differences between the published version and this version may remain and you are advised to consult the published version if you wish to cite from it.

1 **Dependence on temperature and salinity gradients and the injection rate of CO₂ storage**
2 **in saline aquifers with an angular unconformity**

3 Azadeh Pourmalek* S.M Shariatipour

4 Centre for Flow Measurement and Fluid Mechanics, Coventry University, UK

5 *Correspondence: pourmala@uni.coventry.ac.uk

6 **Abstract**

7 An unconformity surface is a type of interface between an aquifer and a caprock. It refers to a
8 buried erosional or non-depositional surface that separates two strata of different ages,
9 indicating that sediment deposition has not been continuous. A high or low-permeability layer
10 may exist just above or below the unconformity surface. The high-permeability layer could be
11 the result of the weathering and erosion of the older layer, or the deposition of coarse-grained
12 sediments on top of the unconformity surface. The effect of this interface on CO₂ dissolution
13 in brine was investigated by running a range of 2D models and considering different injection
14 scenarios. By examining different injection scenarios using two models for comparative
15 analysis (one with and one without a high-permeability layer), the results provide a good
16 hypothesis of the effects of pressure and migration distance on CO₂ dissolution. Although the
17 high-permeable layer creates a pathway for the further migration of CO₂, the models without a
18 high-permeable layer have tended to predict a higher CO₂ dissolution in almost all the injection
19 scenarios. In addition, the sensitivity of CO₂ dissolution to aquifer parameters was examined,
20 such as temperature and salinity gradients. Models with and without temperature and salinity
21 gradients were compared and the importance of these parameters on the prediction of CO₂
22 storage was determined. Another significant result is that under higher injection scenarios, the
23 models show significant sensitivity to temperature and salinity gradients. However, for lower

24 injection rates the sensitivity of the dissolved CO₂ to temperature and salinity gradients is
25 almost negligible.

26 **Keywords:** CO₂ storage. Deep saline aquifer. Unconformity. Temperature gradient. Salinity
27 gradient

28

29 **1. Introduction**

30 New and robust scientific evidence has provided a solid causal link between anthropogenic
31 activity and global warming over the past 50 years. The composition of the atmosphere is
32 expected to continue changing throughout the 21st century. This is now referred to as the
33 anthrosphere (IPCC 2005; Stern 2006).

34 Carbon capture and storage (CCS) is one of the measures that can considerably reduce CO₂
35 emissions into the atmosphere. Three possible CO₂ storage location types are abandoned oil
36 and gas reservoirs, deep un-mineable coal beds and deep saline aquifers. The main points to
37 consider each of these sites are their suitability for permanent CO₂ containment and the extent
38 to which the injected CO₂ could leak into the atmosphere or groundwater (Bachu et al. 1993).
39 The most suitable and globally available short-term option for CO₂ storage is deep saline
40 aquifers (Bachu et al. 1993). The global CO₂ storage capacity of these geological formations is
41 estimated to range from 400 to 10,000 Gt CO₂ (Davison et al. 2001). Their storage capacities
42 make them a significant option and an ideal candidate to be deployed as part of a mitigation
43 policy to reduce the CO₂ burden (Nordbotten et al. 2005).

44 Reservoirs are complex systems and deep formations undergo different tectono-sedimentary
45 evolution through geological years (Song et al. 2014). There is a number of different potential
46 trapping mechanisms exist to store CO₂ in geological media. CO₂ has a lower density compared
47 to the brine in an aquifer and is a buoyant fluid. Therefore, following its injection into a saline

48 aquifer, the CO₂ will move upward under buoyancy to reach a barrier where its migration is
49 prevented by fine-grained rocks (mainly shale) and evaporates, with small pore throat radii in
50 comparison with a reservoir. The CO₂ will then spread out underneath the barrier and move
51 laterally, depending on the caprock and aquifer interface. Consequently, the injected CO₂ is
52 retained primarily at the top surface interval (Nilsen et al. 2012). Therefore, prior to considering
53 a site for CO₂ storage, evaluating the properties of an aquifer and its caprock interface is crucial
54 and has been previously investigated by Shariatipour et al. (2014; 2016a), Nilsen et al. (2012)
55 and Goater et al. (2013).

56 The morphology between the aquifer and the caprock is determined by sedimentological setting
57 and structural deformation. It has a significant effect on the migration paths and the storage of
58 CO₂ (Shariatipour et al. 2016b). An unconformity surface is a type of interface between the
59 aquifer and caprock which refers to a buried erosional or non-depositional surface separating
60 two strata of different ages. Different authors have proposed several trap classifications.
61 However, there is general agreement on three broad categories of trap which are stratigraphic,
62 structural or a combination of both (Biddle, Wielchowsky 1994). Stratigraphic traps are often
63 formed by stratigraphical processes at the time of sediment deposition (Biddle & Wielchowsky
64 1994). Unconformities are a type of stratigraphic trap and play a crucial role in trapping oil and
65 gas. Therefore, they can similarly provide a stratigraphical trap for storing CO₂ as a mitigation
66 action. Categories of unconformity include angular unconformity, disconformity,
67 paraconformity and non-conformity.

68 An angular unconformity is the most common and most recognisable among unconformities.
69 After a period of deformation of older sediments, tilted layers have been subjected to erosion.
70 Subsequently, a younger sediment has been deposited on top. Just above or just below the
71 unconformity surface, there could be a high-permeability or low-permeability layer. The high-
72 permeability layer could be the result of the weathering and erosion of the older layer of the

73 unconformity surface or the deposition of coarse-grained sediments on top of the unconformity
74 surface (Swierczek 2012). Shariatipour et al. (2016b) investigated the effects of the
75 unconformity surface on the storage capacity and security of CO₂. They showed that an
76 unconformity model with a high-permeability layer at the caprock and aquifer interface can
77 contribute to pressure diffusion through the reservoir.

78 In their research, Cao et al. (2005) concluded that in the Permian petroleum system (in the
79 north-west margin of the Junggar Basin, China), hydrocarbons migrate vertically alongside
80 faults and laterally alongside the unconformity surface. In addition, several unconformity
81 surfaces exist in the Sikeshu sag of the Junggar basin. Among them, the unconformity surface
82 at the bottom of the Palaeogene is one of the main migration pathways. It suggests that the
83 unconformity surface can act as an efficient medium for fluid transportation (Gao et al. 2013).
84 Fengjun et al. (2001) investigated the sedimentological characteristics of the Zhuhai and
85 Zhujiang Formations (again in China) and specified that sandstone with good porosity and
86 permeability deposited on the unconformity surface acts as the main migration conduit and
87 provides lateral connectivity for generated oils. Studies of Belfast Bay in the western Gulf of
88 Ontario by Rogers et al. (2006) showed that as a conductive layer, the coarse-grained
89 unconformity between Pleistocene glacial-marine mud and Holocene mud may permit gas to
90 migrate towards the field's margins. Therefore, fluid migration can be restricted across the
91 unconformity surface or just into particular areas, but unrestricted fluid migration can also be
92 permitted across the surface. Both conditions depend on the properties of the unconformity
93 surface and therefore on the process involved in creating the unconformities initially. In this
94 research, the effects of the existence or non-existence of this high-permeability layer on CO₂
95 dissolution is investigated, considering different reservoir parameters including temperature,
96 salinity and injection rate.

97 The supercritical CO₂ flow and storage in deep saline aquifers is a complex, two-phase flow in
98 porous media (Song et al. 2015). As mentioned above, CO₂ can be sequestered in deep saline
99 aquifers. CO₂ and brine are miscible fluids and subsequently, the CO₂ dissolves in brine. The
100 composition and concentration level of dissolved salt in brine differs around the world. Sodium
101 chloride is the main dissolved solid in the saline aquifers. Freshwater typically has less than
102 1000 mg/L total dissolved salt (TDS), dense brine has more than 100,000 mg/L TDS and sea
103 water has about 35,000 mg/L TDS (Oldenburg 2007). Normally, the formation salinity in
104 sedimentary basins gradually increases with depth, with this increase generally being linear,
105 over thousands of metres vertically. The rate of increase ranges from 50 to 300 mg/L/m
106 (Dickey 1969).

107 The equilibrium temperature of the rock and brine that make up the aquifer also changes
108 linearly with depth. The temperature of the subsurface formation depends on a geothermal
109 gradient in that specific region. The degree of temperature increase with depth can be low in a
110 tectonic subduction zone (where tectonic plates meet), to very high along island arcs and
111 volcanic areas (Peacock 1996; Saemundsson et al. 2009). Furthermore, the geothermal gradient
112 can differ noticeably across a region. For instance, in the North Sea, the gradient varies from
113 18°C/km south of Norway to more than 40°C/km in the Central Graben off the Danish coast,
114 with an average of 29°C/km (Harper 1971; Evans 1974). In a sedimentary basin, the
115 temperature gradient varies from 10°C/km to 50°C/km (Koide et al. 1995) and according to
116 Holloway (2008); the typical gradient is between 25-30°C/km.

117 The consequence of the increased temperature is that the density and viscosity of the formation
118 water decrease significantly. As the pressure in the aquifer increases with depth, the density
119 and viscosity increases even with a consequent increase in temperature, but by a less significant
120 amount. The largest increase in density and viscosity is generally observed by an increase in
121 the amount of dissolved solids (TDS) (Bachu and Adam 2003). The pressure, temperature and

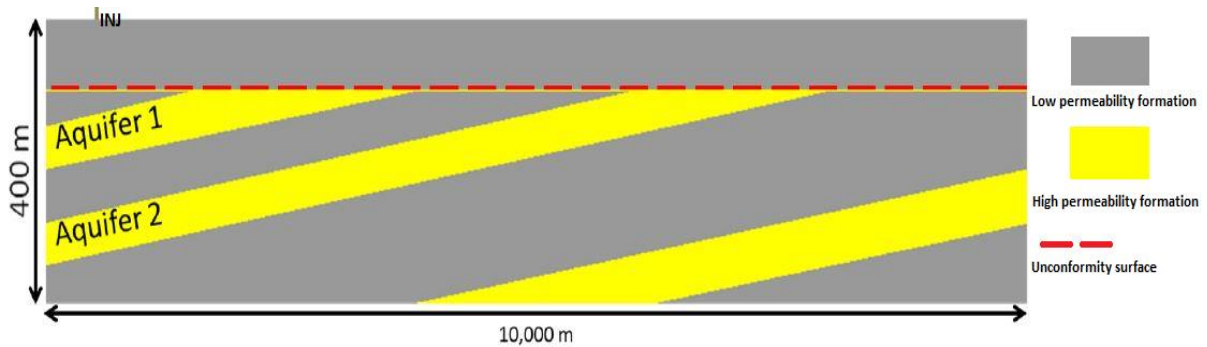
122 salinity of aquifers have significant effects on the ultimate CO₂ solubility in the water phase
123 and the aquifer's storage capacity (Bachu and Adams 2003). The solubility of CO₂ in water
124 increases with pressure (Spycher et al. 2003; Spycher and Pruess (2005; 2010)) and decreases
125 with temperature and water salinity increase (IPCC 2005). Nordbotten et al. (2005) classified
126 different basins with regard to the degree of geothermal gradient and surface temperature.
127 These are categorised as cold basins (a geothermal gradient of 25°C and a surface temperature
128 of 10°C) and warm basins (a geothermal gradient of 45°C and a surface temperature of 20°C),
129 respectively.

130 In most cases, the vertical variations in salinity and temperature are ignored in CO₂ simulations.
131 Therefore, the original vertical profile of salinity and temperature remains almost unchanged
132 during the simulation period (Shariatipour et al. 2016b). In other words, in previous simulation
133 studies, constant reservoir salinity and temperature were considered. However, as mentioned
134 above, normally formation salinity and temperature in sedimentary basins gradually increase
135 with depth. Therefore, it is necessary to consider temperature and salinity gradient in CO₂
136 storage modelling. In this research, the modelling exercise undertakes the comparative effect
137 of constant reservoir salinity and temperature against variation in these parameters, to assess
138 the relative effect on CO₂ dissolution and migration in saline aquifers with unconformity.

139 **2. Model description**

140 Numerical simulation is progressively applied for forecasting fluid flow in the porous media
141 (Mousavi Nezhad et al. 2011). Although Numerical simulation software have inadequacies
142 such as long computing time (Song et al. 2014), they are crucial for modeling the CO₂ flow in
143 the porous media for CCS technology. A reliable and precise model must completely reflect
144 all the mechanisms involved in the system (Mousavi Nezhad et al. 2011). Fluid flow is
145 significantly affected by the properties of the domain through which the process happens
146 (Mousavi Nezhad et al. 2011). The base model used to investigate the effects of salinity and

147 temperature gradients and the effects of an unconformity surface on CO₂ dissolution was an
 148 angular unconformity 2D Model with a length of 10 Km, a thickness of 400 m and a width of
 149 100 m, which was discretized into 100× 445 ×1 cells. The aquifers were assumed to be
 150 homogeneous and the model boundaries assumed to be closed. One injection well was located
 151 on the left-hand side of the modelled aquifer. The maximum bottom hole pressure was limited



152

Fig. 1 Angular Unconformity (2D) model as a base case (Shariatipour et al. 2016b).

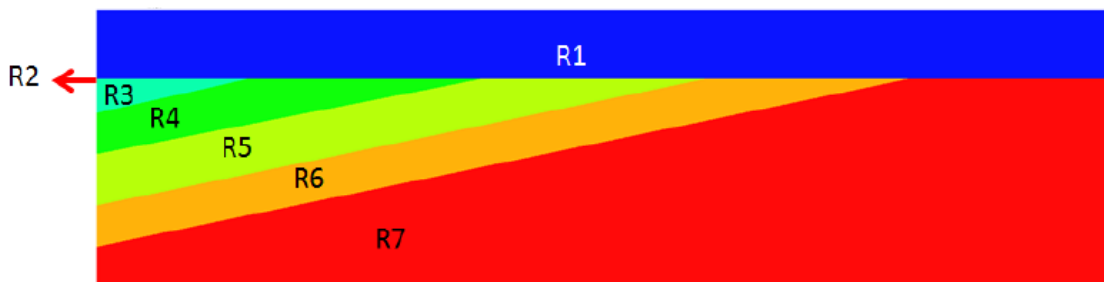


Fig. 2 Seven regions of the model: (R1)-caprock, (R2)-interface between caprock and aquifer (unconformity surface), (R3)-low- permeability layer above aquifer 1, (R4) aquifer 1, (R5)-low- permeability layer between aquifer 1 and 2, (R6)- aquifer2, (R7)- low-permeability layer below aquifer2. R refers to regions (Shariatipour et al. 2016b).

153 to 229 bars. To investigate the effect of an unconformity surface, different injection rate
 154 scenarios were taken into consideration as the pressure did not reach the restrictive bottom-
 155 hole pressure. The injector was closed after 50 years and the simulation was continued for a
 156 further 200 years. The base model is shown in Figure 1 and was taken from Shariatipour et al.
 157 (2016b). All models were constructed using Schlumberger's Petrel Modelling© software, and
 158 the reservoir models were input into the Schlumberger ECLIPSE© compositional reservoir
 159 simulator with the CO2STORE option. The model was divided into seven regions (shown in
 160 Figure 2) with the porosity and permeability of each region and model properties shown in

161 table 1 and 2, respectively. The relative permeability curves used in this model (Smith et al.
 162 2012) is shown in Figure 3.

163

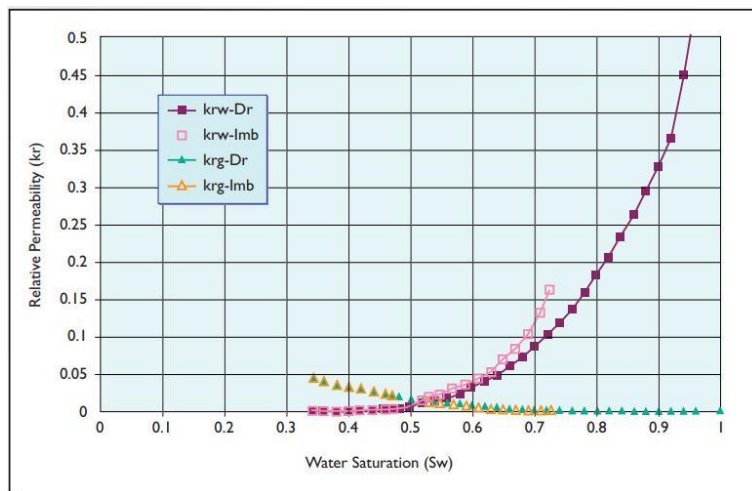
Table 1 Properties of each region.

Formation	Porosity	Permeability (mD)
Caprock (R1)	10%	1E-06
Unconformity interface (R2)	25%	1000
Low permeable layer above aquifer 1(R3)	10%	1E-06
Aquifer 1(R4)	25%	1000
Low permeable layer between aquifer 1 and 2 (R5)	10%	1E-06
Aquifer 2 (R6)	25%	1000
164 Low permeable layer below aquifer 2 (R7)	10%	1E-06

165

Table 2 Model properties.

Model parameters	Value
Rock Compressibility (bar^{-1})	5×10^{-5}
Fluid Compressibility (bar^{-1})	3×10^{-5}
Initial mole fraction	CO ₂ H ₂ O NaCl
	0.0 0.967 0.033
Datum depth (m)	900
Pressure at datum depth (bar)	90
166 Maximum relative permeability to CO ₂	0.0654



167

Fig. 3 The relative permeability curves (Smith et al. 2012).

168

169

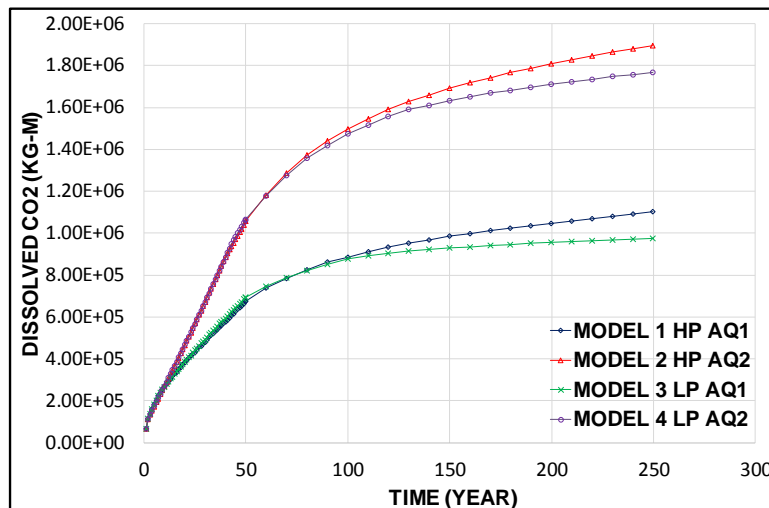
170 3. Effect of a high-permeability layer on CO₂ dissolution

171 Model 1 had a high-permeability layer at the unconformity surface with permeability of the
172 saline aquifers (1000 mD). In this model, CO₂ was injected at the bottom of Aquifer 1. Model
173 2, as with model 1, had a high-permeability layer but CO₂ was injected through a perforation
174 at the bottom of Aquifer 2. Models 3 and 4 did not have the high-permeability layer and the
175 unconformity surface had permeability equal to the caprock. The only difference between these
176 two models was the location of the perforation. In Model 3, CO₂ was injected at the bottom of
177 Aquifer 1 but in Model 4, CO₂ was injected at the bottom of Aquifer 2. Different injection
178 scenarios (3×10^3 , 4×10^3 , 5×10^3 , 7×10^3 , 20×10^3 , 35×10^3 , 50×10^3 and 70×10^3 SM³/day) were
179 taken into consideration to investigate the effects of the properties of the interface between the
180 caprock and the aquifer; and therefore, the distance migrated and the pressure on CO₂
181 dissolution. To do so, these eight different injection scenarios were set for each model. This
182 meant that at the end, 32 models were constructed.

183 Given that the distance from the perforation at the bottom to the caprock of Aquifer 1 was less
184 than that of Aquifer 2, it was therefore predictable that CO₂ injected into Aquifer 1 would reach
185 the top much sooner. Moreover, in Models 1 and 2, CO₂ could migrate laterally through the
186 permeable layer, as it plays a role as a conductive layer which connects the two aquifers.
187 Therefore, the injected CO₂ could reach the second storage formation. In Models 3 and 4, when
188 the high-permeable conductive layer does not exist, the CO₂ lateral migration was restricted
189 and the injected CO₂ could not reach the second storage formation. Therefore, the properties
190 of the caprock and aquifer interface play an important role as they provide a pathway for CO₂
191 to migrate laterally or to restrict its pathway.

192 Figure 4 compares the dissolved CO₂ in all four models when the injection rate was relatively
193 low (5×10^3 SM³/day). CO₂ dissolution in Models 2 and 4 was higher than for Models 1 and 3

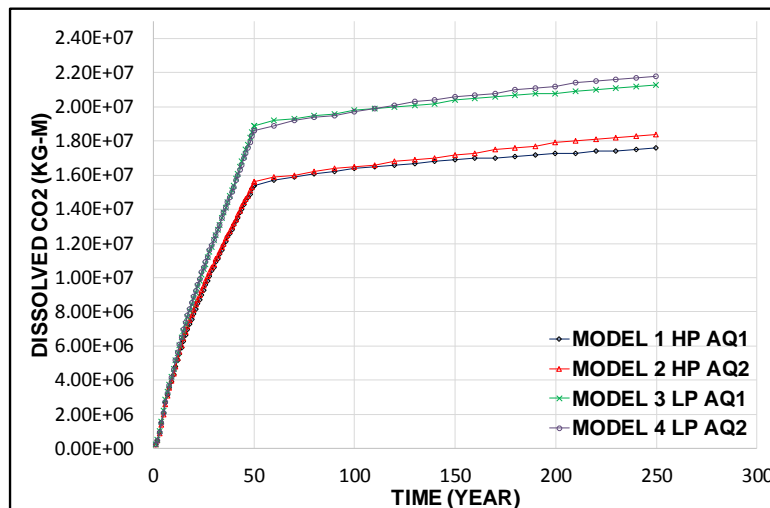
194 (40%). CO₂, which is less dense than brine, migrates upward until it reaches the top seal. The
 195 distance that the CO₂ migrates in Aquifer 2 was far more than in Aquifer 1 and therefore it was
 196 in contact with the brine for longer. The dissolution trapping mechanism then plays a far more
 197 active role. Regarding the dissolved CO₂ in the models with the high-permeable conductive
 198 layer (Models 1 and 2) and the models with the low-permeable layer (Models 3 and 4), the CO₂
 199 dissolution results using Model 1 were higher than for Model 3, while Model 2 were higher
 200 than Model 4 (6%). This is due to the fact that the CO₂ migrates laterally through the high-
 201 permeable layer and starts to use another aquifer as a second storage formation. In other words,
 202 these two aquifers are connected by the high-permeable layer. The obvious difference starts at
 203 the 50 years post-injection period as is clear from the figure. During the injection period (50
 204 years), there is no noticeable difference existing between the models with a high-permeable
 205 layer and those with a low-permeable layer, since during this period, the CO₂ has not reached
 206 the conductive layer.



207 Fig.4 Dissolved CO₂ in relatively low injection rate (5×10^3 SM³/day). HP refers to high-permeability and LH refers to Low-permeability.

208 Figure 5 compares the dissolved CO₂ for the four models when the injection rate is relatively
 209 high (70×10^3 SM³/day). Most noticeable in this figure is that more CO₂ is dissolved in Models
 210 3 and 4 with a low-permeable layer and that the difference is apparent from the middle of the

211 injection period. This is due to the fact that for higher injection rates, the pressure increases
 212 and more CO₂ dissolution in brine is triggered by that increase. At the end of the post-injection
 213 period, the highest CO₂ dissolution is seen in the results of Model 4 with a low-permeable layer
 214 at the unconformity surface when the CO₂ was injected into Aquifer 2. This is because on the
 215 one hand, the CO₂ migrates further in Aquifer 2 until it reaches the caprock so there is time for
 216 more brine and CO₂ interaction. On the other hand, the formation pressure is higher in the
 217 closed aquifer when the unconformity interface becomes part of the caprock and no conductive
 218 layer exists. The difference observed between the model's results with the CO₂ injection at the
 219 bottom of Aquifer 1 or Aquifer 2 is not significant. Therefore, in the presence of a low-
 220 permeability layer, as long as the pressure does not reach the pressure constraint, the higher
 221 injection rate plays a more effective role in CO₂ dissolution. The least dissolution had occurred
 222 using Model 1. Therefore, more CO₂ dissolution occurs in the closed model with a greater
 223 distance to the caprock.



224 Fig.5 Dissolved CO₂ in relatively high injection rate (70×10^3 SM³/day). HP refers to high-permeability and LH refers to low-permeability.

225

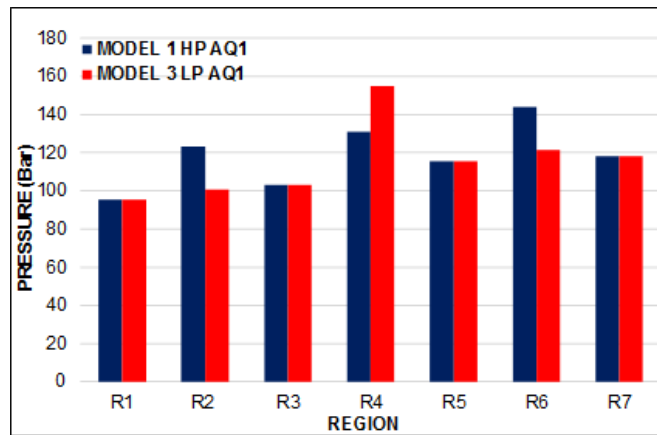


Fig.6 Average pressure when CO₂ is injected at the bottom of Aquifer 1 (R as region).

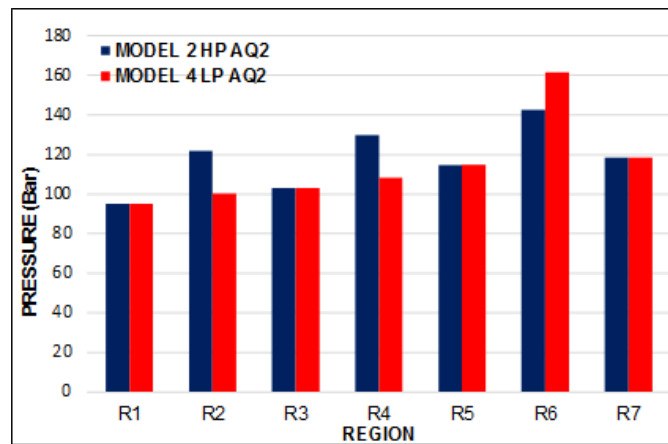


Fig.7 Average pressure when CO₂ is injected at the bottom of Aquifer 2 (R as region).

226

227

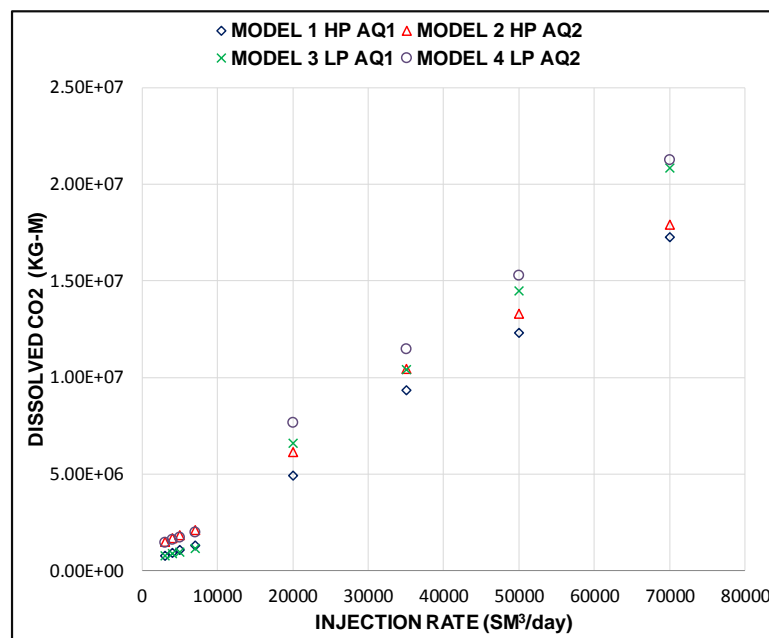
228

229 In both figures (6 & 7 above), no significant difference is observable in pressure in the low-
 230 permeable regions even after injecting CO₂. This is because free CO₂ does not enter these
 231 regions to increase the pressure. In Figure 6, the highest pressure is experienced in Aquifer 1
 232 (region 4) of Model 3. This is because CO₂ was directly injected into this aquifer and also, as
 233 for the closed model, the conductive layer does not exist for CO₂ migration and pressure
 234 diffusion. The average pressure in Aquifer 2 (region 6) of Model 3 does not change since the
 235 lateral connectivity is restricted. Therefore, free CO₂ cannot migrate laterally to fill Aquifer 2
 236 and increase the pressure. Hence in Model 3, the average pressure in Aquifer 2 is lower than
 237 Aquifer 1. However, the pressure in Aquifer 2 (region 6) of Model 1 is increased, since CO₂

238 enters this aquifer through the high-permeability layer. The high-permeability layer contributes
239 to the pressure diffusion from Aquifer 1 to Aquifer 2 (Shariatipour et al. 2016b).

240 In Figure 7, the average pressure is shown when CO₂ is injected into Aquifer 2. As expected,
241 the highest average pressure is observable in Aquifer 2 for the simulations using Model 4 for
242 the reasons explained above.

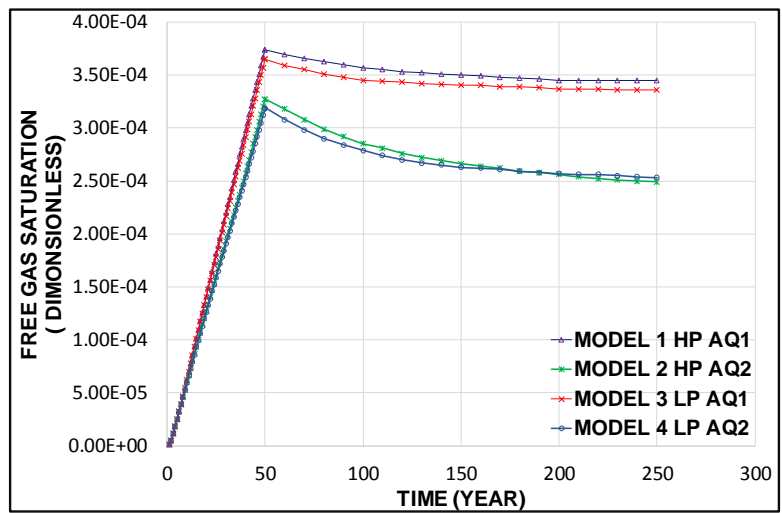
243 Figure 8 shows the amount of dissolved CO₂ predicted by all the models at the end of the post-
244 injection period. For the lowest injection rate (3×10^3 SM³/day), the lowest amount of dissolved
245 CO₂ is observed in Model 3 (7.37×10^5 Kg-M). The highest dissolution occurs using Model 2
246 (1.46×10^6 Kg-M), again due to the longer migration distance and therefore, the higher CO₂ and
247 brine interaction time. For the highest injection rate studied (70×10^3 SM³/day), the lowest
248 amount of CO₂ dissolution occurs using Model 1 (1.73×10^7 Kg-M). The highest CO₂
249 dissolution occurs with Model 4 (2.12×10^7 Kg-M) because of the combined effects of the
250 greater pressure increase and the longer migration distance.



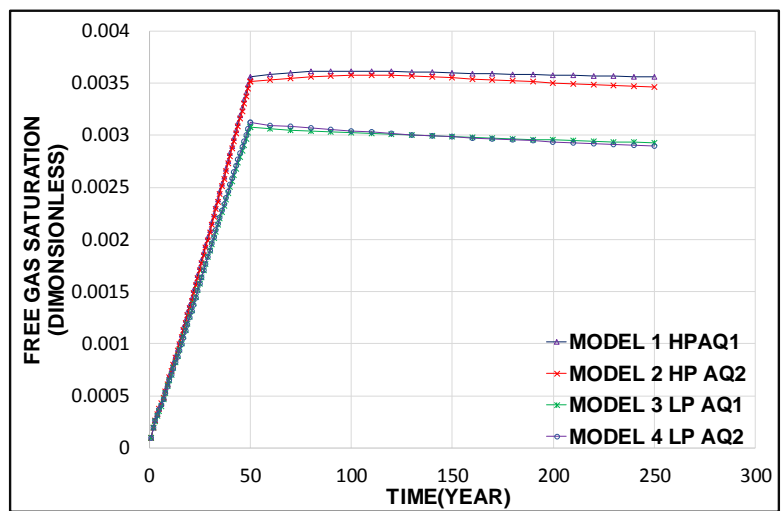
251 Fig. 8 Amount of dissolved CO₂ at the end of the post injection period for all injection scenarios.

252 Figure 9 demonstrates the free gas saturation for a rather low injection rate of 5×10^3 SM³/day
253 in all four models. The least free gas is observed using Models 2 and 4 with the perforation at

254 the bottom of Aquifer 2, since more CO₂ was dissolved for these models because of the highest
 255 interaction between the brine and the CO₂. The highest amount of free gas is observed using
 256 Models 1 and 3 with less dissolved CO₂ in the water phase. Figure 10 shows the free gas
 257 saturation at a higher injection rate of 70×10³ SM³/day. The lowest free gas saturation is seen
 258 using Model 4, since more CO₂ was dissolved in this model as a result of the combined effects
 259 of the higher pressure and longer migration distance. Once the CO₂ dissolves in the water phase,
 260 it can no longer exist as a free gas. Therefore, it is not possible for the CO₂ to travel upwards
 261 under buoyancy; hence, the security and effectiveness of the storage will be improved.



262 Fig.9 Free gas saturation (dimensionless) at 5×10³ SM³/day injection rate.



263 Fig.10 Free gas saturation (dimensionless) at 70×10³ SM³/day
 264 injection rate.

265 **4. Effect of salinity and temperature gradient on CO₂ dissolution**

266 The temperature of the subsurface formation depends on the geothermal gradient in that
267 specific region. Temperature changes linearly by depth. Normally, the salinity of the
268 formations water in sedimentary basins gradually increases by increasing the depth. In this part,
269 the effects of constant reservoir temperature, temperature gradient, constant reservoir salinity
270 and salinity gradient are investigated.

271 **4.1 Temperature effect**

272 In order to observe the effect of reservoir temperature on CO₂ dissolution, different temperature
273 values were first assigned to the models (31°C, 35°C, 40°C, 45°C, 50°C). In this step, the
274 temperature gradient was not taken into consideration. As expected, the field of dissolved CO₂
275 in the water phase is seen to decrease as the temperature increases (Figure 11). By increasing
276 temperature, the solubility of the CO₂ in brine decreases. Furthermore, the viscosity of the brine
277 decreases as temperature increases. In the CO₂ and water displacement system, relative
278 permeability, irreducible saturation and capillary pressure play important roles. These
279 characteristics, along with other factors, rely on the interfacial tension between the formation
280 water and the CO₂. In a situation when salinity and pressure are constant (similar to the research
281 conditions), the interfacial tension between the CO₂ and the formation water increases with an
282 increasing temperature (Bachu and Bennion 2009). Moreover, a generally inverse relationship
283 exists between the interfacial tension of the CO₂ and the formation water and the solubility of
284 CO₂ in the water phase.

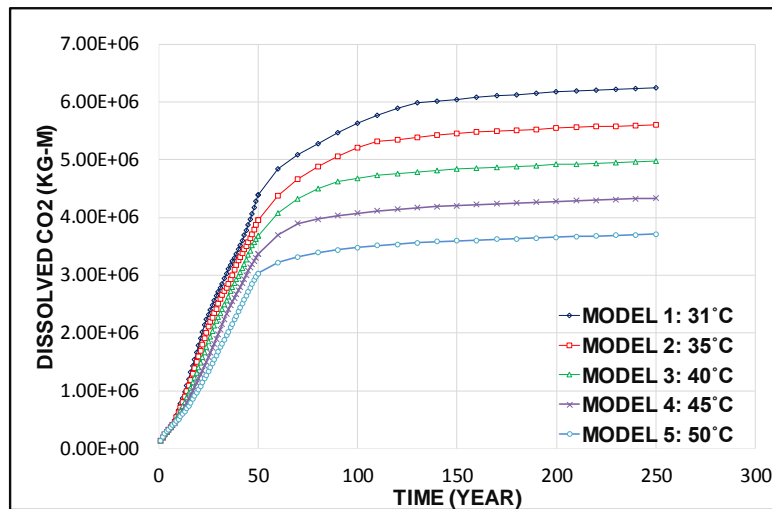


Fig.11 Effect of constant reservoir temperature on CO₂ dissolution.

285

286

287 4.1.1 Effect of temperature gradient on CO₂ dissolution

288 Two models were constructed in order to investigate the effects of the temperature gradient.

289 The geothermal gradient was created by assigning different values of temperature to a different

290 depth. For the temperature gradient of 2°C/100m, at the datum depth, the temperature was

291 assigned to be 33°C. Then, the temperature was increased (2°C/100m) linearly with the depth.

292 For the temperature gradient of 5°C/100m, at the datum depth, the temperature was assigned to

293 be 60°C. Again, the temperature was increased (5°C/100m) linearly with the depth.

294 One of these models had a temperature gradient of 2°C/100m, which is a cold basin, while the

295 other model had a higher temperature gradient of 5°C/100m, which is a warm basin. Figure 12

296 demonstrates the effects of the two different geothermal gradients on CO₂ dissolution.

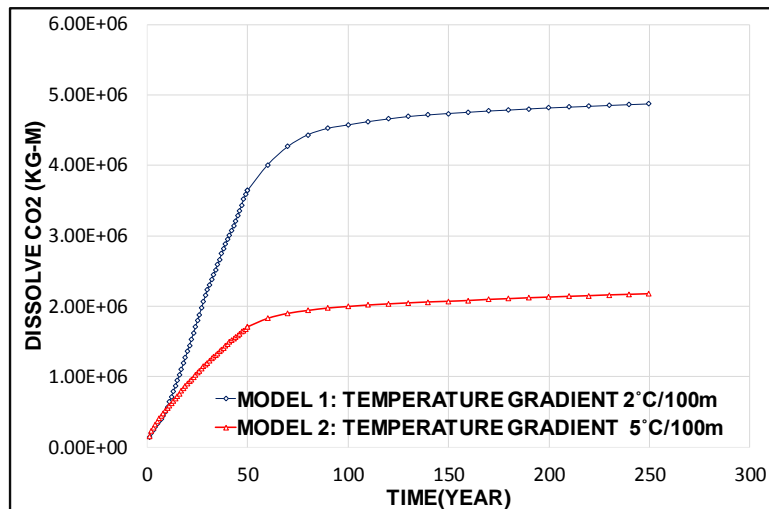


Fig.12 Effect of temperature gradient on CO₂ dissolution.

297

298 Obviously noticeable from this figure is that in the model with the higher temperature gradient
 299 (5°C), the field of dissolved CO₂ in the formation water drastically decreased. This is because
 300 for higher temperature gradients, the solubility of CO₂ in the water phase is less than its
 301 solubility in lower temperature gradients. In other words, brine in cooler basins can contain
 302 more CO₂ than warmer ones. Furthermore, the difference in dissolved CO₂ in these two
 303 gradients starts at the beginning of the injection period, since CO₂ was injected at the bottom
 304 of the aquifer where the temperature have the highest value. This fact had a major influence on
 305 the CO₂ dissolution from the start of the simulation.

306 At the end of the injection period, the amount of dissolved CO₂ in the water phase is 5.61E+06
 307 Kg-m in the model with the constant reservoir temperature of 35°C. In the model with the
 308 temperature gradient of 2°C/100m, the amount of dissolved CO₂ in the water phase is 4.87E+06
 309 Kg-m indicating a significant decrease (12%) in CO₂ dissolution. Figure 13 demonstrates this
 310 difference. Hence, ignoring the temperature gradient leads to overestimating the amount of
 311 dissolved CO₂ in the aquifer and the storage capacity.

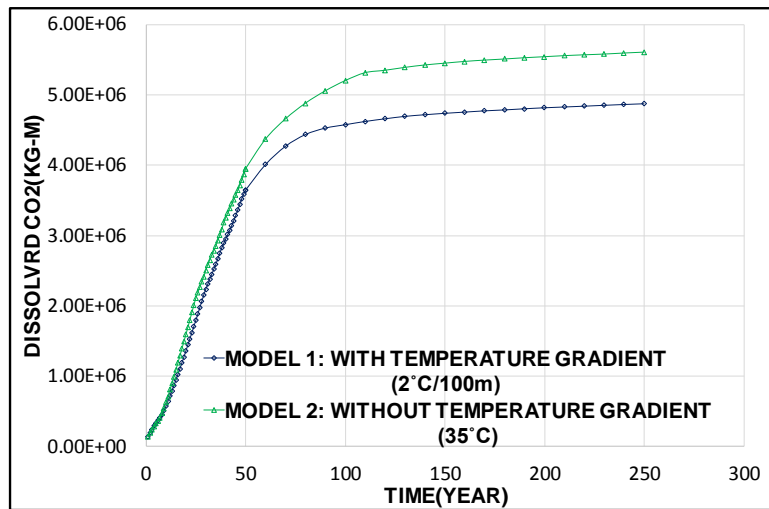


Fig.13 Comparison between Models with and without a temperature gradient.

312

313 4.2 Salinity effects

314 In order to examine the impacts of formation water salinity on CO₂ dissolution, five models
 315 with salinity levels of 10,000 mg/L, 75,000 mg/L, 100,000 mg/L, 165,000 mg/L, and 200,000
 316 mg/L were generated. In these models, the reservoir temperature was assumed to be constant
 317 (35°C).

318 As predicted, the amount of dissolved CO₂ in the aquifer decreases as the salinity increases
 319 (Figure 14). The brine density increases by increasing the salt concentration. Hence, due to the
 320 density difference between the formation water and the CO₂, the buoyancy forces play a more
 321 active role. Consequently, the interaction between the brine and the CO₂ is reduced. Therefore,
 322 the degree of the solubility trapping as a major trapping mechanism is dependent on salinity.
 323 By increasing brine salinity, the degree of solubility trapping is decreased (Johnson et al. 2004).

324 In order to improve the effectiveness of this type of trapping mechanism and minimise the
 325 upward migration of CO₂ under buoyancy, the salinity of the formation water must be
 326 considered. Aquifers with low salinities are freshwater resources (<1000 mg/L) and need to be
 327 conserved. Thus, the salinity of the formation water needs to be moderate.

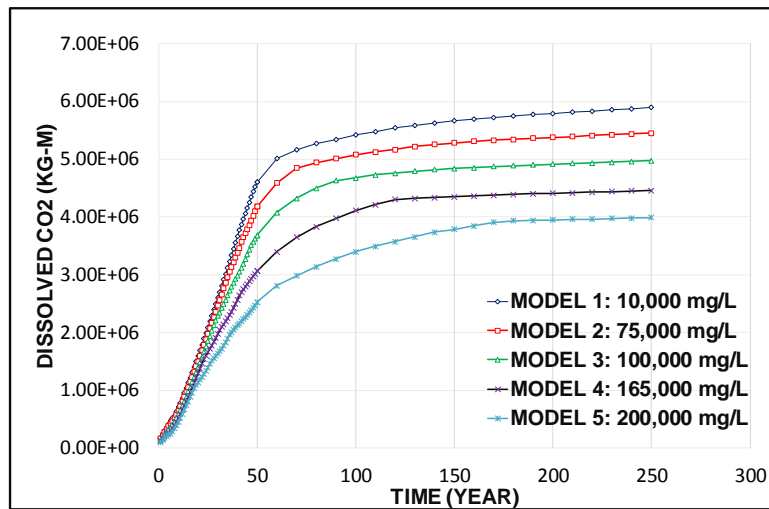


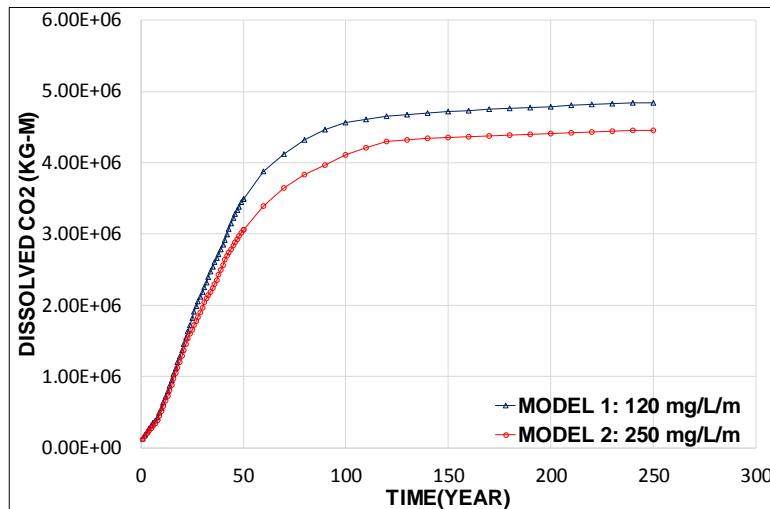
Fig.14 Effect of constant reservoir salinity on CO₂ dissolution.

328

329 4.2.1 Effect of salinity gradient on CO₂ dissolution

330 Dickey (1969) demonstrated that salinity changes with depth at a rate of 50 mg/L to 300 mg/L
 331 per m. The overall composition (CO₂, H₂O, and NaCl) of the formation was modified with
 332 depth to examine and evaluate the effect of the salinity gradient on the solubility of CO₂. The
 333 mole fraction at datum depth was 0.0, 0.967 and 0.033 for CO₂, H₂O and NaCl respectively.
 334 For example, Model 1 had a salinity gradient of 120 mg/L/m. Therefore, the mole fractions of
 335 0.0, 0.96 and 0.04 were assigned to the model at a depth of 1100. Model 2 used a salinity
 336 gradient of 250 mg/L/m. Therefore, the mole fractions of 0.0, 0.95 and 0.05 were assigned to
 337 the model at a depth of 1100. These models used a constant reservoir temperature of 35°C.

338 Figure 15 demonstrates the effect of salinity gradient on CO₂ dissolution in the water phase. It
 339 is evident from this figure that the CO₂ dissolution in the water phase decreases by increasing
 340 the salinity of the formation water with depth.



341

Fig.15 Effect of the salinity gradient on CO₂ dissolution.

342

At the end of the injection period, the amount of dissolved CO₂ in the water phase is 4.46E+06

343

Kg-m in the model with the constant reservoir salinity. The amount of dissolved CO₂ in the

344

water phase is 4.67E+06 Kg-m in the model with the salinity gradient of 250 mg/L/m.

345

Comparing the models with and without the salinity gradient, but at a close average salinity,

346

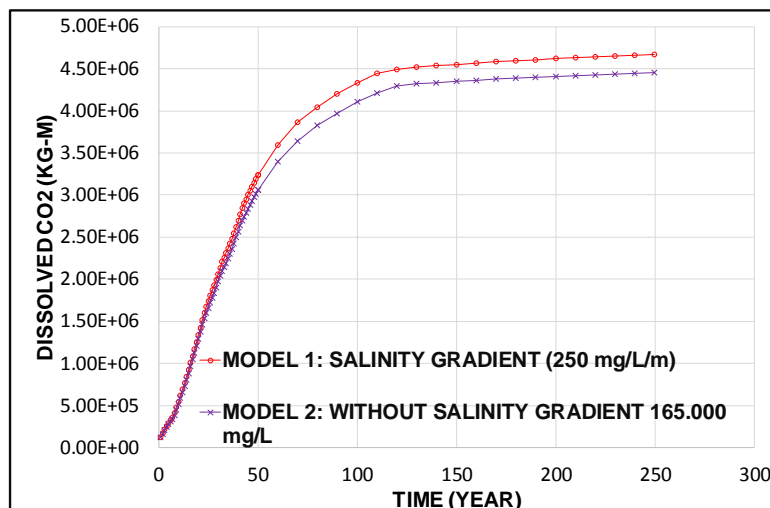
demonstrates the difference (4%) and the importance of considering the salinity gradient for

347

the amount of CO₂ dissolution. Figure 16 shows this comparison. Ignoring the salinity gradient

348

leads to underestimating the amount of dissolved CO₂ in the aquifer.

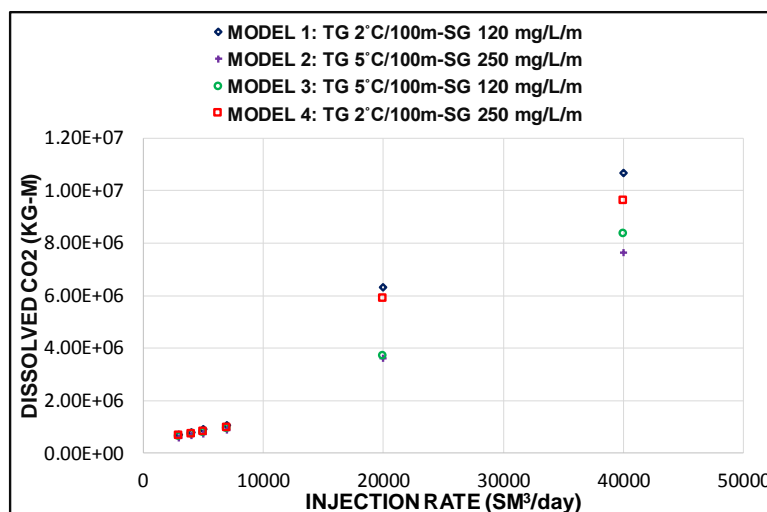


349

Fig.16 Comparison between Models with and without the salinity gradient.

350 **5. The combined effect of salinity gradients, temperature gradients and injection rates**
351 **on CO₂ dissolution**

352 24 models were constructed in order to investigate the combined effects of salinity gradients,
353 temperature gradients, and different injection scenarios, using two salinity gradients, two
354 temperature gradients and six different injection rates. Figure 17 demonstrates the amount of
355 dissolved CO₂ in the water phase in these 24 model simulations for the 200 years post-injection
356 period. Models with low salinity and temperature gradients have the capacity to dissolve the
357 most CO₂ and models with high salinity and temperature gradients have the capacity to dissolve
358 the least. From this figure, it is clear that for lower CO₂ injection rates of 3×10^3 , 4×10^3 , 5×10^3
359 and 7×10^3 SM³/day, the effects of salinity gradients and temperature gradients on CO₂
360 dissolution are almost negligible. However, at higher injection rates of 20×10^3 and 40×10^3
361 SM³/day; this effect becomes noticeable. Higher injection rates trigger the models to be more
362 sensitive to higher salinity and temperature gradients, due to the consequential pressure increase
363 which is not the case in lower injection rates. In addition, for the low injection rates, the injected
364 CO₂ does not reach those depths with substantially different temperature and salinity gradients.
365 Therefore, the effect of variation in salinity and temperature on the amount of dissolved CO₂ is
366 insignificant.



367

Fig.17 Amount of dissolved CO₂ in models with a different temperature gradient, salinity gradient and a different injection rate.

368 **6. Conclusion**

369 The main intention of CO₂ storage is to maximize the amount of CO₂ that can be injected into
370 an aquifer and minimise the leakage potential as a mitigation option.

371 While investigating the unconformity surface as a type of aquifer and caprock interface on CO₂
372 dissolution it was observed:

373 1. When the injection rate is rather low, the distance travelled by the CO₂ plays a
374 significant role towards increasing the total amount of CO₂ becoming dissolved. A
375 longer distance means increased interaction between the brine and the CO₂ and
376 therefore a higher dissolution in the water phase. When CO₂ is injected at the bottom
377 of Aquifer 2, the amount of dissolved CO₂ is higher due to the greater distance to the
378 top of the interval. Moreover, CO₂ dissolution in aquifers with a high-permeable
379 conductive layer is higher than for aquifers without the high-permeable layer at lower
380 injection rates. This layer provides a pathway to other storage formations. Hence, CO₂
381 travels a longer distance which results in a higher CO₂ dissolution.

382 2. When the injection rate is relatively high, dissolution is increased in closed aquifers
383 with a low-permeable layer. The highest dissolved CO₂ is observed using the model
384 with a low-permeable layer at an unconformity surface and when the CO₂ was injected
385 at the bottom of Aquifer 2. This is due to the fact that for higher injection rates, the
386 pressure builds up and more CO₂ will be dissolved in the water phase. Moreover, more
387 dissolution occurs when the pathway to the caprock is longer, as the brine and CO₂
388 interaction is increased. Therefore, in the presence of a low-permeability layer,
389 injection rates play a more effective role in CO₂ dissolution, as long as the pressure
390 does not reach the pressure constraint.

- 391 3. Less free gas was also observed in the aquifers with the higher amount of CO₂
392 dissolution in the water phase. A higher amount of free CO₂ in the aquifers means a
393 higher leakage potential and therefore a reduction of CO₂ storage security.
- 394 4. Overall, it is crucial to have precise injection rate and also the well and perforation
395 location to maximise the storage potential and security of a CO₂ storage project.
- 396 5. CO₂ dissolution is affected by aquifer salinity and reservoir temperature. In warmer
397 aquifers, less CO₂ will be dissolved into the water phase. This is also the case for
398 aquifers with a higher salinity. As expected, the amount of CO₂ dissolved in the water
399 phase is reduced with an increase in temperature and salinity. In summary, these results
400 indicate that warmer aquifers and aquifers with high salinity have a lower capacity to
401 dissolve CO₂. However, the decrease of solubility is more drastic for the model
402 simulations using higher temperature gradients than in the models with salinity
403 gradients. The low solubility of CO₂ in high-salinity brines and high-temperature
404 formations leaves more CO₂ in the gas phase, which reduces storage security. In
405 addition, since the difference in the amount of dissolved CO₂ between models with and
406 without temperature and salinity gradients is significant, considering the temperature
407 and salinity gradient is crucial when selecting a formation for CO₂ storage. Ignoring
408 them may cause overestimating or underestimating the storage capacity.
- 409 6. One of the interesting results was that for a lower injection rate, the effect of salinity
410 and temperature gradients on CO₂ dissolution is almost negligible. However, at higher
411 injection rates, the models' sensitivity to temperature and salinity gradient is significant
412 due to higher pressure and a longer migration distance.
- 413 7. In sum, it is essential to consider salinity and temperature gradients in modelling studies
414 as they have large effects on the amount of dissolved CO₂ in the brine and hence the
415 storage capacity and security.

416 Since CO₂ storage efficiencies are related to the size of the connected aquifers, the formation
417 heterogeneity and the CO₂ injection strategy, conducting heterogeneous models to investigate
418 its effects on CO₂ dissolution are recommended for future studies.

419 **References**

- 420 1. Bachu, S. and Adams, J. (2003) 'Sequestration of CO₂ in Geological Media in Response
421 to Climate Change: Capacity of Deep Saline Aquifers to Sequester CO₂ in Solution'.
422 *Energy Conversion and Management* 44 (20), 3151-3175.
- 423 2. Bachu, S. and Bennion, D.B. (2008) 'Interfacial tension between CO₂, freshwater, and
424 brine in the range of pressure from (2 to 27) MPa, temperature from (20 to 125)°C, and
425 water salinity from (0 to 334 000) mg· L⁻¹'. *Journal of Chemical & Engineering*
426 *Data*, 54(3), 765-775.
- 427 3. Bachu, S., Gunter, W. and Perkins, E. (1993) 'Aquifer Disposal of CO₂: Hydrodynamic
428 and Mineral Trapping'. *Energy Conversion and Management* 35 (4), 269-279.
- 429 4. Biddle, K. T. and Wielchowsky, C. C. (1994) 'Hydrocarbon Traps'. *Memoirs-American*
430 *Association of Petroleum Geologists*, 219-219.
- 431 5. Cao, J., Zhang, Y., Hu, W., Yao, S., Wang, X., Zhang, Y. and Tang, Y. (2005) 'The
432 Permian hybrid petroleum system in the northwest margin of the Junggar Basin,
433 Northwest China. *Marine and Petroleum Geology*, 22(3), 331-349.
- 434 6. Davison, J., Freund, P. and Smith, A. (2001) 'Putting Carbon Back into the Ground'.
435 *IEA Greenhouse Gas R&D Programme* 28.
- 436 7. Dickey, P.A. (1969) 'Increasing Concentration of subsurface brines with
437 depth. *Chemical Geology*, 4(1-2), 361-370.
- 438 8. Evans, T.R. and Coleman, N.C. (1974). 'North Sea geothermal gradients'. *Nature*, 247
439 (5435), 28-30.

- 440 9. Fengjun, N., Sitian, L., Hua, W., Xinong, X., Keqiang, W. and Meizhu, J. (2001)
441 ‘Lateral migration pathways of petroleum in the Zhu III sub-basin, Pearl River Mouth
442 basin, South China Sea. *Marine and Petroleum Geology*, 18(5), 561-575.
- 443 10. Gao, X., Liu, L., Jiang, Z., Shang, X. and Liu, G. (2013) A Pre-Paleogene unconformity
444 surface of the Sikeshu Sag, Junggar Basin: Lithological, geophysical and geochemical
445 implications for the transportation of hydrocarbons. *Geoscience Frontiers*, 4(6), 779-
446 786.
- 447 11. Goater, A.L., Bijeljic, B. and Blunt, M.J. (2013) ‘Dipping open Aquifers—the effect of
448 top-surface topography and heterogeneity on CO₂ storage efficiency. *International
449 Journal of Greenhouse Gas Control*, 17, 318-331.
- 450 12. Harper, M.L. (1971) ‘Approximate geothermal gradients in the North Sea
451 basin. *Nature*, 230(5291), 235-236.
- 452 13. Holloway, S. (2009) ‘Storage capacity and containment issues for carbon dioxide
453 capture and geological storage on the UK continental shelf. *Proceedings of the
454 Institution of Mechanical Engineers, Part A: Journal of Power and Energy*, 223(3),
455 239-248.
- 456 14. IPCC (2005) *IPCC Special Report on Carbon Dioxide Capture and Storage*. In: METZ,
457 B., DAVIDSON, O., DE CONINCK H.C., LOOS, M., MEYER, L.A. (Eds.), Prepared
458 by Working Group III of the Intergovernmental Panel on Climate Change. Cambridge
459 University Press, Cambridge, UK/New York, NY, USA, 442.
- 460 15. Johnson, J.W., Nitao, J.J. and Knauss, K.G. (2004) ‘Reactive transport modelling of
461 CO₂ storage in saline aquifers to elucidate fundamental processes, trapping mechanisms
462 and sequestration partitioning’. *Geological Society, London, Special
463 Publications*, 233(1), 107-128.

- 464 16. Koide, H., Takahashi, M., Tsukamoto, H. and Shindo, Y. (1995) 'Self-Trapping
465 Mechanisms of Carbon Dioxide in the Aquifer Disposal'. *Energy Conversion and*
466 *Management* 36 (6), 505-508.
- 467 17. Mousavi Nezhad, M., Javadi, A.A. and Abbasi, F. (2011) 'Stochastic finite element
468 modelling of water flow in variably saturated heterogeneous soils. *International*
469 *Journal for Numerical and Analytical Methods in Geomechanics*, 35(12), 1389-1408.
- 470 18. Mousavi Nezhad, M., Javadi, A.A. and Rezania, M. (2011) 'Modeling of contaminant
471 transport in soils considering the effects of micro-and macro-heterogeneity. *Journal of*
472 *hydrology*, 404(3-4), 332-338.
- 473 19. Nilsen, H.M., Syversveen, A.R., Lie, K.A., Tveranger, J. and Nordbotten, J.M. (2012)
474 Impact of top-surface morphology on CO₂ storage capacity. *International Journal of*
475 *Greenhouse Gas Control*, 11, pp.221-235.
- 476 20. Nordbotten, J.M., Celia, M.A. and Bachu, S. (2005). 'Injection and storage of CO₂ in
477 deep saline Aquifers: Analytical solution for CO₂ plume evolution during
478 injection'. *Transport in Porous Media*, 58(3), 339-360.
- 479 21. Oldenburg, C.M. (2007) 'Migration mechanisms and potential impacts of CO₂ leakage
480 and seepage'. *Carbon Capture and Sequestration Integrating Technology, Monitoring,*
481 *and Regulation*, 127-146.
- 482 22. Peacock, S.M. (1996) Thermal and petrologic structure of subduction
483 zones'. *Subduction top to bottom*, 119-133.
- 484 23. Rogers, J.N., Kelley, J.T., Belknap, D.F., Gontz, A. and Barnhardt, W.A. (2006)
485 'Shallow-water pockmark formation in temperate estuaries: a consideration of origins
486 in the western gulf of Maine with special focus on Belfast Bay. *Marine*
487 *Geology*, 225(1), 45-62.

- 488 24. Saemundsson, K., Axelsson, G. and Steingrímsson, B. (2009) ‘Geothermal systems in
489 global perspective’. *Short Course on Exploration for Geothermal Resources, UNU*
490 *GTP*, 11.
- 491 25. Shariatipour, S. M., Pickup, G. E. and Mackay, E. J. (2016a) ‘Simulations of CO₂
492 storage in aquifer models with top surface morphology and transition
493 zones’. *International Journal of Greenhouse Gas Control*, 54, 117-128.
- 494 26. Shariatipour, S. M., Pickup, G. E. and Mackay, E. J. (2016b). ‘Investigation of CO₂
495 torage in a saline formation with an angular unconformity at the caprock
496 interface. *Petroleum Geoscience*, 22(2), 203-210.
- 497 27. Shariatipour, S.M., Pickup, G.E. and Mackay, E.J. (2014) ‘The Effect of
498 Aquifer/Caprock Interface on Geological Storage of CO₂’. *Energy Procedia*, 63, 5544-
499 5555.
- 500 28. Smith, M., Campbell, D., Mackay, E. and Polson, D., 2011. CO₂ aquifer storage site
501 evaluation and monitoring. *Heriot Watt University, Edinburgh, ISBN*, pp.978-0.
- 502 29. Song, H., Huang, G., Li, T., Zhang, Y. and Lou, Y. (2014) Analytical model of CO₂
503 storage efficiency in saline aquifer with vertical heterogeneity’. *Journal of Natural Gas*
504 *Science and Engineering*, 18, 77-89.
- 505 30. Song, Z., Song, H., Cao, Y., Killough, J., Leung, J., Huang, G. and Gao, S. (2015)
506 ‘Numerical research on CO₂ storage efficiency in saline aquifer with low-velocity non-
507 Darcy flow’. *Journal of Natural Gas Science and Engineering*, 23, 338-345.
- 508 31. Spycher, N., Pruess, K. and Ennis-King, J. (2003) ‘CO₂-H₂O mixtures in the geological
509 sequestration of CO₂. I. Assessment and calculation of mutual solubilities from 12 to
510 100 °C and up to 600 bar’. *Geochimica et Cosmochimica Acta*, 67(16), 3015-3031.
- 511 32. Stern, N.H. (2006) *The Economics of climate change: the Stern review*. Cambridge:
512 Cambridge University Press.

513 33. Swierczek, M. (2012) *Role of unconformities in controlling clastic reservoir*
514 *properties: insights from adopting a multidisciplinary approach* (Doctoral dissertation:
515 Heriot-Watt University.

516